Since January 2020 Elsevier has created a COVID-19 resource centre with free information in English and Mandarin on the novel coronavirus COVID-19. The COVID-19 resource centre is hosted on Elsevier Connect, the company's public news and information website.

Computers in Biology and Medicine 146 (2022) 105598

Contents lists available at ScienceDirect

Computers in Biology and Medicine

journal homepage: www.elsevier.com/locate/compbiomed

Computational studies evidenced the potential of steroidal lactone to disrupt surface interaction of SARS-CoV-2 spike protein and hACE2

Ajay Yadav [1], Monu Dinesh Ojha [1], P. Hariprasad [*]

Centre for Rural Development and Technology, Indian Institute of Technology Delhi, Hauz Khas, New Delhi, 110016, India

ARTICLE INFO

Keywords:
Hydrogen bond occupancy
Spike-receptor binding domain
Withalongolide A
Binding energy
Protein-protein interaction

ABSTRACT

The critical event in severe acute respiratory syndrome coronavirus 2 (SARS-CoV-2) pathogenesis is recognition of host cells by the virus, which is facilitated by protein-protein interaction (PPI) of viral Spike-Receptor Binding Domain (S-RBD) and Human Angiotensin Converting Enzyme 2-Receptor (hACE2-R). Thus, disrupting the interaction between S-RBD and hACE2-R is widely accepted as a primary strategy for managing COVID-19. The purpose of this study is to assess the ability of three steroidal lactones (SL) (4-Dehydrowithaferin A, Withaferin A, and Withalongolide A) derived from plants to disrupt the PPI of S-RBD and hACE2-R under two conditions (CON–I and CON-II) using *in-silico* methods. Under CON–I, 4-Dehydrowithaferin A destabilizing the interactions between S-RBD and hACE2-R, as indicated by an increase in binding energy (BE) from −1028.5 kJ/mol (control) to −896.12 kJ/mol 4-Dehydrowithaferin A exhibited a strong interaction with S-RBD GLY496 with a hydrogen bond occupancy (HBO) of 37.33%. Under CON-II, Withalongolide A was capable of disrupting all types of PPI, as evidenced by an increased BE from −913 kJ/mol (control) to −133.69 kJ/mol and an increased distance (>3.55 nm) between selected AAR combinations of S-RBD and hACE2-R. Withalongolide A formed a hydrogen bond with TYR453 (97%, HBO) of S-RBD, which is required for interaction with hACE2-R's HIS34. Our studies demonstrated that SL molecules have the potential to disrupt the S-RBD and hACE2-R interaction, thereby preventing SARS-CoV-2 from recognizing host cells. The SL molecules can be considered for additional *in-vitro* and *in-vivo* studies with this research evidence.

1. Introduction

Coronaviruses (CoV; order Nidovirales, family Coronaviridae, subfamily Coronavirinae) have been implicated in transmitting infectious diseases in both humans and animals [1]. However, a global outbreak of a respiratory illness [Coronavirus disease (COVID-19)] caused by newly discovered coronavirus variants, SARS-CoV-2, threatened human existence by claiming 54.76 lakhs lives until January 5, 2022 [2]. The WHO designated Alpha, Beta, Gamma, Delta, and Omicron as SARS-CoV-2 variants of concern [3].

The genetic material of SARS-CoV-2 is a positive-sense single-stranded RNA virus (approximately 30,000 bases) that codes for both structural (spike, nucleocapsid, membrane, and envelope) and non-structural (proteases and RNA dependent RNA polymerases) proteins [4,5]. Researchers worldwide have delineated the molecular mechanism of SARS-CoV-2 pathogenesis using a polyphasic approach. Crown-like spikes cover the virus's outer surface, composed of heterotrimeric transmembrane glycoproteins (S glycoprotein), which is critical for early detection and facilitates viral entry into the host cell. The hACE2-R attached to the host cell's outer surface serves as the actual viral recognition site, facilitating the interaction of the SARS-CoV-2 S-RBD and thus initiating the pathogenesis process [6].

The increased virulence of SARS-CoV-2 over SARS-CoV can be attributed to its increased affinity for hACE2-R due to variation in the amino acid sequence of S-RBD [7–10]. Several attempts have been made to block the S-RBD using small molecules, peptides, ACE2 fractions, convalescent serum from individuals recovered from COVID-19 infection, and polyclonal/monoclonal antibodies, among others [11,12] in order to decrease the affinity between S-RBD and hACE2-R. However, success with small molecules is limited due to the involvement of large interacting surface between S-RBD and hACE2-R in PPI. Additionally, the increased transmissibility and virulence of the SARS-CoV-2 variants of concern, namely Alpha, Beta, Gamma, Delta, and Omicron, are primarily due to a favourable spike protein mutation exacerbates the

* Corresponding author.
E-mail addresses: phari@iitd.ac.in, phimprovement.iitd@gmail.com (P. Hariprasad).
[1] Both authors have contributed equally to this work.

https://doi.org/10.1016/j.compbiomed.2022.105598
Received 21 October 2021; Received in revised form 9 March 2022; Accepted 2 April 2022
Available online 13 May 2022

situation. As a result, it is assumed that these variants will overcome the effect of currently available spike protein blocking vaccines or peptides.

With the rapid global spread of SARS-CoV-2, numerous antiviral drugs and therapies became available to alleviate the additional burden of COVID-19. Remdesivir (inhibitor of viral RNA-dependent RNA polymerase) was the only drug approved by US Food and Drug Administration for COVID-19 treatment [13]. Monoclonal antibodies (REGEN-COV, Bamlanivimab, Tocilizumab, and Etesevimab), convalescent plasma therapy, renal replacement therapies, and immune modular are reported as effective [14]. Nevertheless, following the successful development of vaccines (Covishield, Covaxin, COVOVAX, mRNA-1273, Sputnik V, Ad26.COV2.S, and others) and the implementation of a global vaccination program, morbidity and mortality decreased significantly [15]. However, the threat remains, as the new SARS-CoV-2 "Omicron" variant of concern (B.1.1.529) spreads faster than the wild type and other variants.

Due to the diversity of secondary metabolites at the structural and functional levels, plants are considered a critical source of drugs. Natural herbs have recently gained increased importance as potential antiviral agents due to their minimal adverse effects [16–19]. In 12 randomized controlled trials, traditional Chinese medicine demonstrated significant improvements in clinical symptoms while lowering COVID-19 mortality and recurrence rate [20,21]. Similarly, other clinical trials conducted on adults with early and mild flu symptoms using 39 herbal medicines revealed the potential of *Althaea officinalis*, *Commiphora molmol*, *Glycyrrhiza glabra*, *Hedera helix*, and *Sambucus nigra* as *anti*-COVID-19 [22]. According to Kanjanasirirat et al. [23], *Boesenbergia rotunda* extract and its pure compound panduvatin significantly reduced SARS-CoV-2 infectivity in Vero-E6 cells, with IC_{50} values of 3.62 μg/ml and 0.81 μM, respectively. Similarly, several small molecules of plant origin have been reported for their antiviral, prophylactic, and therapeutic activity against SARS-CoV-2 [24,25]. Salvianolic acid (a dimer of caffeic acid) [26], cepharanthine (bisbenzylisoquinoline alkaloid), colforsin (a forskolin derivative for *Coleus forskohlii*) and ingenol (from *Euphorbia peplus*) [27] were all reported to inhibit virus entry into the host cell. In contrast, baicalin (flavone glycoside) [28] was reported to be 3CLpro inhibitor of SARS-CoV-2. Emodin (anthraquinone) was identified as one of the best drug candidate with *anti*-SARS-CoV-2 activity in Calu-3 (human lung cell) in an *in-silico* and cell-based assay [29]. Berbamine, a naturally occurring alkaloid found in Chinese herbal medicine, inhibited SARS-CoV-2-Spike entry into Vero-E6 cells and further decreased the viral yield [30].

The purpose of this study is to identify plant secondary metabolites (PSM), with a particular emphasis on SL, that have a higher affinity for S-RBD and can disrupt the early interaction of S-RBD with hACE2-R via MDS. SLs are primarily found in the *Withania* spp., a major source of modern medicine [31]. The withanolides, a class of naturally occurring SL, have been implicated in a variety of therapeutic effects, including anticancer, immunomodulation, cardio-respiratory, memory enhancer enhancement, diuretic, mood elevator, rejuvenator, anti-epileptic, stress reliever, endurance enhancer, anti-ageing, antioxidant, hypocholesterolemic, and hypoglycemic properties [32–37]. Through disruption of the viral S-RBD and hACE2 interaction, an *in-vitro* study of withanone-enriched *Withania somnifera* extract was reported to be *anti*-SARS-CoV-2 [38]. Kumar et al. [39] demonstrated that withaferin A and withanone have transmembrane serine protease and main protease inhibitory properties using an *in-silico* method. Withaferin A, which possesses strong antiviral and immunomodulatory properties, has also been demonstrated to be a potent inhibitor of the SARS-CoV2 Main protease (M^{pro}), making it a critical molecule to monitor in this pandemic situation [40]. On the other hand, Withanolides have been shown to increase IFN γ and IL-2 cytokine production, skewing the immune response towards T-helper1 (Th1) rather than Th2 cell type [41,42].

Computational methods, artificial intelligence, and machine learning [43] are indispensable tools for drug development. The computational method expedites the selection of likely therapeutic molecules via high-throughput screening. It lowers the cost of experiments and allows for further evaluation of potential lead molecules through *in-vitro* and *in-vivo* studies. The majority of previous studies aimed to identify small molecules capable of inhibiting the interaction of S-RBD with hACE2-R [44–46], which is constrained by the protein's rigidity. Molecular dynamic simulation is superior to MD because it creates a native environment in which the ligand can interact with the target protein, simulating realistic conditions. Additionally, the results can be analyzed using Molecular Mechanics Poisson-Boltzmann Surface Area (MMPBSA), which incorporates electrostatic energy, van der Waal energy, solvent accessible surface area (SASA) energy, and polar solvation energy. Lower MMPBSA values indicate a more stable energetically advantageous interaction and vice versa. Thus, the purpose of the current study is to better understand the ability of selected SL to disrupt the S-RBD and hACE2-R interaction via detailed MDS studies.

2. Materials and methods

2.1. Preparation of ligands and proteins

3D structure data file (SDF files) and canonical SMILES of three SL molecules (4-Dehydrowithaferin A (PubChem Id: 165541), Withaferin A (PubChem Id: 265237) and, Withalongolide A (PubChem Id: 56649343) were retrieved from the PubChem database (https://pubchem.ncbi.nlm.nih.gov). The crystal structure of SARS-CoV-2 S-RBD bound to hACE2-R (PDB ID: 6M0J) (2.45 Å) was downloaded from Research Collaborator for Structural Bioinformatics (RCSB) Protein Data Bank (PDB) (RCSB, http://www.rcsb.org). CHIMERA 1.13.1 [47] was used to clean the protein complex, and stereo-chemical quality checks and energy minimizations were done using a Swiss-Pdb viewer to get the optimal 3D structure [48].

2.2. Molecular dynamics simulations (MDS)

Ensemble docking (8 clusters) [49] was performed against S-RBD, and the best pose with least BE was chosen for MDS (Sup. Table 1). Molecular dynamic simulation studies were used to determine the SL's PPI disruption strength, as well as protein's stability and flexibility in the presence/absence of SL. Two conditions were used to subject the three SL molecules to all-atom MDS. The crystal structure PPI between S-RBD to hACE2-R was retained in CON–I, and the test molecule was introduced based on the docking pose with the least BE on S-RBD. The molecules ability to disrupt previously established AAR interactions between S-RBD and hACE2-R was assessed. Under CON-II, the distance between S-RBD and hACE2-R was increased using CHIMERA 1.13.1 tools, and the test molecule was introduced based on the docking pose that contained least BE on S-RBD.

Additionally, the complex was allowed to interact with hACE2-R. The MDS analysis was carried out using the latest Gromacs-5.0.7 suite [50–52]. The CHARMM36 all-atom force field was chosen for protein [53]. To obtain ligand topology, the Swiss-PARAM modelling web server was used [54].

In the absence and presence of ligand, the prepared S-RBD and hACE2-R complex were solvated in TIP3P water model in a cubic box with 1.2 nm distance between the protein surface and the box boundary [55]. Energy minimization was done by the steepest descent minimization algorithm in the aqueous phase. Verlet cutoff scheme [56] and Particle mesh Ewald (PME) were incorporated to control the non-bonded and the long-range electrostatic interaction [50,57]. Equilibration was achieved in two stages: NVT first, then NPT. The LINCS algorithm was incorporated to retain all H-bond constraints [58,59]. System pressure 1 bar and temperature 300k were regulated using the Parrinello-Rahman pressure coupling method and Berendsen temperature coupling, respectively [60,61]. All the MDS was carried for the 50 ns in triplicates, and trajectory was saved at every two fs using

Table 1
Interactions energy and Binding energies of the selected steroidal lactones and SARS-CoV-2 Spike Protein RBD complex.

Name and PubChem ID	VDW (kJ/mol)	PSE (kJ/mol)	EE (kJ/mol)	SASA (kJ/mol)	BE (kJ/mol)
Condition-I					
Control	−311.64 ± 26.3	650.65 ± 156.50	−1325.90 ± 61.02	−41.61 ± 3.99	−1028.5 ± 149.61
4-Dehydrowithaferin A (165541)	−183.23 ± 28.1	440.82 ± 206.13	−1123.45 ± 72.16	−24.88 ± 4.35	−896.12 ± 12.77
Withaferin A (265237)	−168.02 ± 19.8	418.93 ± 157.54	−1070 ± 69.58	−26.12 ± 3.84	−845.26 ± 151.08
Withalongolide A (56649343)	−204.05 ± 23.6	284.91 ± 123.70	−1055.10 ± 56.84	−26.41 ± 4.49	−1000.65 ± 110.6
Condition-II					
Control	−331.70 ± 18.5	727.52 ± 140.19	−1266.47 ± 62.22	−43 ± 3.2	−913.66 ± 137.11
4-Dehydrowithaferin A (165541)	−55.91 ± 2.56	275.12 ± 13.78	−978.83 ± 8.39	−9.83 ± 0.46	−769.62 ± 16.75
Withaferin A (265237	−213.63 ± 18.8	439.21 ± 133.99	−1315.61 ± 53.45	−26.51 ± 3.86	−1116.55 ± 140.29
Withalongolide A (56649343)	−9.22 ± 7.9	555.93 ± 2539.67	−679.81 ± 112.51	−0.59 ± 3.39	−133.69 ± 2556.8

*VDW-Van der Waals interactions, EE-electrostatic energy, PSE- Polar solvation energy, SASA energy, BE-binding energy.

High-Performance Computing Facility (HPC), Indian Institute of Technology Delhi, India. The workflow of MDS and data analysis is provided as Sup. Fig. 1.

2.3. Free energy of binding calculation (MMPBSA)

The free BE of the S-RBD and hACE2-R complex in the absence and presence of ligands under CON–I and CON-II was calculated by using the g_mmpbsa toolkit [62,63]. The last 10 ns converged snapshots at every 100 ps were incorporated to analyze binding free energy, polar solvation energy, van der Waals energy, Solvent accessible surface area (SASA) energy, and electrostatic energy.

2.4. RMSD, RMSF, Rg, SASA, and HBN

Using g_rms tool (least-square fit method), the root means square deviation (RMSD) of the protein backbone was calculated. The root mean square fluctuation (RMSF) of the amino acid residues was calculated by using g_rmsf tool. The radius of gyration (Rg) and total SASA were calculated by gmx_gyrate and gmx_sasa tools, respectively. The average intermolecular hydrogen bond number (HBN) with 3.5 Å distance cutoff was calculated by the gmx_hbond tool. Trajectories were saved, and results were analyzed using Origin (Pro), 2021 software [64].

2.5. Distance measurement between amino acid residues

The most critical parameter to count the effects of the drug on the S-RBD and hACE2-R complex destabilization is the distribution of the distance between their centres of mass (C-alpha atom) at the interface area. An increase in the distance specifies the disruption of PPI. gmx_distance function was used to measure the C-alpha distance of the eight amino acid combinations between S-RBD and hACE2-R (GLY496 - ASP38, GLY446 - GLN42, THR500 - GLY326, GLY502 - GLY354, ASP405 - ALA387, LEU455 - ASP30, ASN487 - PHE28 and PHE486 - LEU79), which cover a wide interacting surface area of S-RBD and hACE2-R. Distance between the amino acid combinations mentioned above was recorded for 50 ns of MDS. The average distance of these amino acid combinations from the last 10 ns MDS were mentioned.

2.6. Hydrogen bond occupancy (HBO)

To understand the involvement of H-bond in maintaining the protein-protein or protein-ligand interaction, HBO (%) was analyzed using the H-bond VMD plugin tool [65] for the last 10 ns MDS with a 5% cutoff.

2.7. In-silico prediction of ADME/Tox properties

Drug likeness, Pharmacokinetic [absorption, distribution, metabolism, excretion (ADME) and toxicology properties of SL were studied using SwissADME [66] and pkCSM-pharmacokinetics web tool [67].

3. Results and discussion

4- Dehydrowithaferin A, Withaferin A, and Withalongolide A are the SL molecules found in many Solanaceae plants. Withaferin A is the first member of the ergostane type withanolides. 4-Dehydrowithaferin A and Withalongolide A are derivatives of Withaferin A where oxidation at C-4 and C-27 positions leads to the formation of 4- Dehydrowithaferin A, and addition of hydroxyl group at 19 position leads to Withalongolide A (Sup. Fig. 2) [68]. Withanolides, the active ingredients of *W. somnifera*, have displayed promising results in managing COVID-19. The significant biological action of *W. somnifera* is rendered by Withanolide D, Withaferin-A, Withanoside X, and Withanoside I–VII [69]. Withaferin A has been reported to have anticancer, angiogenesis inhibitor, anti-inflammatory, antistress, immunomodulatory, antioxidant and anti-ageing properties [70,71]. Whereas 4- Dehydrowithaferin A and Withalongolide A have primarily been investigated for their anticancer activity [46,72,73]. The antiviral activity of 4- Dehydrowithaferin A and Withalongolide A, on the other hand, has not been evaluated.

Computational studies can be used to identify protein-protein interaction disrupting the small molecules by performing MDS and monitoring the position of S-RBD and hACE2-R by measuring the distance between selected amino acids, analyzing the H-bond and other types of interactions, and free BE calculations. As previously stated, MDS were conducted for 50 ns under two conditions. The trajectories were examined using VMD tools [65] and it was determined that none of the molecule was expelled from the protein-protein interface during the simulation period.

Under CON–I, the equilibrium reached in 10 ns without ligand and was maintained throughout the simulation period (Fig. 2). Under the same conditions, it is expected that when a ligand is introduced between two proteins with previously established AAR interactions between AAR of S-RBD and hACE2-R and form new interactions with either/both proteins. As a result, more deviations in the RMSD values were observed in the presence of ligands (Fig. 2). However, initially, both the proteins were physically separated under CON-II to facilitate the ligand to interact with S-RBD protein in the early simulation period. Initially, the control reactions showed greater fluctuations in RMSD values up to 10 ns. Following that, the proteins achieved equilibrium and remained so throughout the simulation period (Fig. 2). The average RMSD values for control under CON–I and CON-II were 0.260 (nm) and 0.405 (nm), respectively (Sup. Table 3). Withaferin A reached equilibrium faster than control and was maintained for 50 ns under both test conditions, with an average RMSD value of 0.458 nm under CON–I and 0.320 nm under CON-II (Sup. Table 3). Whereas 4-Dehydrowithaferin A and Withalongolide A induced significant conformational changes in S-RBD and hACE2-R, as evidenced by increased RMSD values; the same was maintained until the simulation ended without reaching equilibrium. In comparison to CON–I, CON-II resulted in a significant increase in RMSD. This RMSD pattern indicates that 4-Dehydrowithaferin A and Withalongolide A create unfavourable conditions for the interaction of S-RBD and hACE2-R (Fig. 2; Sup. Table 3).

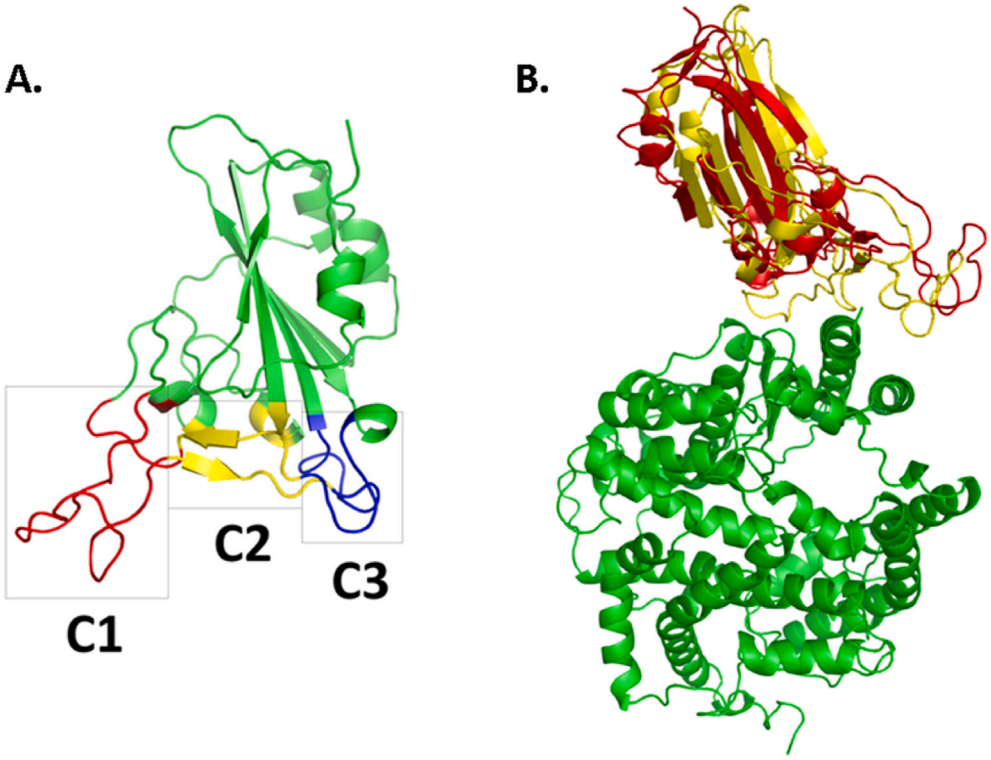

C.

Condition	ASN487–PHE28	ASP405–ALA387	GLY446–GLN42	GLY496–ASP38	GLY502-GLY354	LEU455–ASP30	PHE486–LEU79	THR500-GLY326
I	7.5	9.4	8.5	6.6	4.1	8.4	7.5	6.5
II	13.3	11.2	18.4	12.7	6.7	11.6	15.1	9.9

Fig. 1. A. Cartoon structure showing S-RBD of SARS-CoV-2 highlighted as C1, C2 and C3 region known interact with hACE2-R. B. Position S-RBD on hACE2-R (Green) under CON–I (Yellow) and CON-II (Red) used in the present study. C. Table represents distance (Å) between the selected amino acid residue combinations under CON–I and CON-II.

A similar trend was observed with respect to Rg values in control and SL molecules under CON–I, with average Rg values of 3.19 nm, 3.12 nm, 3.10 nm and 3.15 nm for control, 4-Dehydrowithaferin A, Withaferin A, and Withalongolide A, respectively (Fig. 2; Sup. Table 3). However, with Withalongolide A (average Rg 3.29 nm), increased Rg values and high fluctuation was observed under CON-II (Fig. 2; Sup. Table 3). During the simulation, these properties cause significant changes in the structural conformation of the protein.

Under CON–I, the SASA values (nm^2) ranged between 345 and 390 for control and tested protein-SL complex. The SASA values remained constant under CON-II for the first 20 ns before decreasing with control. The protein-Withalongolide A complex increased to a value of >390 in the final 10 ns of the MDS (Fig. 2; Sup. Table 3). The root mean square fluctuation (RMSF) of AAR was analyzed to determine whether the ligands affect the dynamic behaviour of AAR of S-RBD and hACE2-R. The C1, C2, and C3 regions of the S-RBD (Fig. 1A) are primarily composed of loops and interact with hACE2-R. During the MDS, the high fluctuation in C1, C2, and C3 regions of S-RBD was also observed. Compared to CON–I, the RMSF values of AAR belonging to both proteins were higher under CON-II. S-RBD exhibited the highest RMSF in the presence of Withalongolide A, indicating its instability. Whereas Withaferin A demonstrated a decreased RMSF in comparison to its respective controls, implying that it stabilizes S-RBD (Fig. 3).

3.1. Analysis of distance between selected pair of AAR between S-RBD and hACE2-R

The introduction of ligands under CON–I increased the distance between seven selected AAR combinations. Whereas, the distance between ASP405-ALA387 decreased in the presence of withaferin A and 4-Dehydrowithaferin A, indicating that the spike protein's position may have been shifted, reducing the distance between this amino acid combination (Fig. 5A and B). Whereas, under CON-II, with Withalongolide A and 4-Dehydrowithaferin A, a clear separation of proteins was observed, as

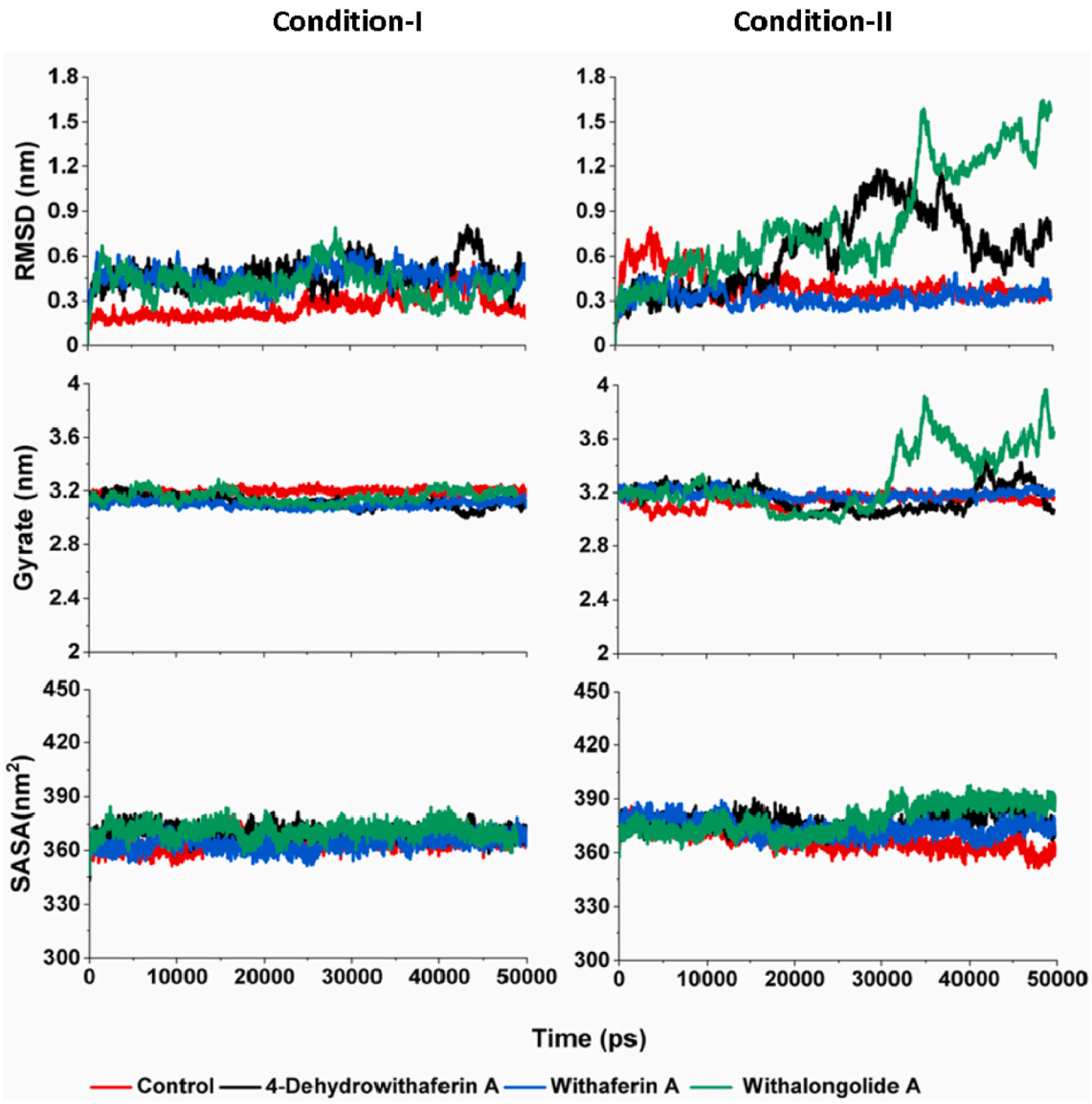

Fig. 2. Root Mean Square Deviation (RMSD) of the S-RBD-hACE2-R complex backbone, Radius of gyration of the S-RBD-hACE2-R complex, and Solvent accessible surface area (SASA) of the hACE2-R-S-RBD complex in presence and absence of ligands under CON–I and CON-II.

evidenced by the increased distance between all AAR combinations studied. In both cases, the distance between the majority of amino acids studied remains unchanged (Fig. 5B). The distance between all the selected amino acid combinations was >3.55 nm and >1.18 nm in the presence of Withalongolide A and 4-Dehydrowithaferin A molecules, respectively, indicating that PPI via H-bond and other types of interactions is likely. The distance between these amino acid combinations was varied between 0.40 and 1.08 nm in control (Fig. 5B). The results obtained demonstrated that Withalongolide A and 4-Dehydrowithaferin A are capable of disrupting the PPI between S-RBD and hACE2-R.

3.2. Analysis of HBO and MMPBSA under CON–I

Throughout the simulation period, the AAR interactions (H-bonds) between S-RBD and hACE2-R were found to be consistent (Fig. 6A). Without the ligand, the total number of H-bond between S-RBD and hACE2-R varied between of 2 and 17 (Average 8.57) over 50 ns simulation period (Sup. Fig. 3). During the final 10 ns of MDS, 11 AAR interactions between S-RBD and hACE2-R were observed in the form of an H-bond (Fig. 6A). TYR505-GLU37 had the highest HBO of 124%, followed by ASN487-TYR83, THR500-ASP355, LYS417-ASP30, and GLY502-LYS353 recorded >70% HBO (Fig. 6A). Whereas, in the presence of4-Dehydrowithaferin A, Withaferin A, and Withalongolide A, the total number of H-bond (Average of 50 ns) between S-RBD and hACE2-R was reduced to 2.41, 4.98 and 2.78, respectively (Sup. Fig. 3). With all three test molecules, a slight bend in the spike protein position was observed as early as 10 ns in the presence of ligands. After 20 ns, the orientation of S-RBD shifted significantly and continued to do so until the end (Fig. 4B, C, 4D). When different simulations frames were analyzed, it was discovered that all the molecules were parallel to S-RBD. SL had ergostane framework facing the C1 and the lactone ring facing the C3 of S-RBD. While all three ligands appear to be visually disrupting the S-RBD and hACE2-R interactions, they were unable to dissociate the two proteins. To substantiate this, the BE was found to have increased from −1028.5 kJ/mol (control) to −896.12 kJ/mol, −845.26 kJ/mol and −1000.65 kJ/mol in 4-Dehydrowithaferin A, Withaferin A and Withalongolide A, respectively (Table 1).

Total AAR interactions were reduced to six in the presence of Withalongolide A. Additionally, HBO of TYR505-GLU37 was reduced to 70%. HBO of LYS417-ASP30, GLY502-LYS353 and TYR453-HIS34, on the other hand, was found to be nearly equivalent to control (Fig. 6A). Six AAR interactions (ASN487-GLN24, ASN501-TYR41, ALA475-SER19,

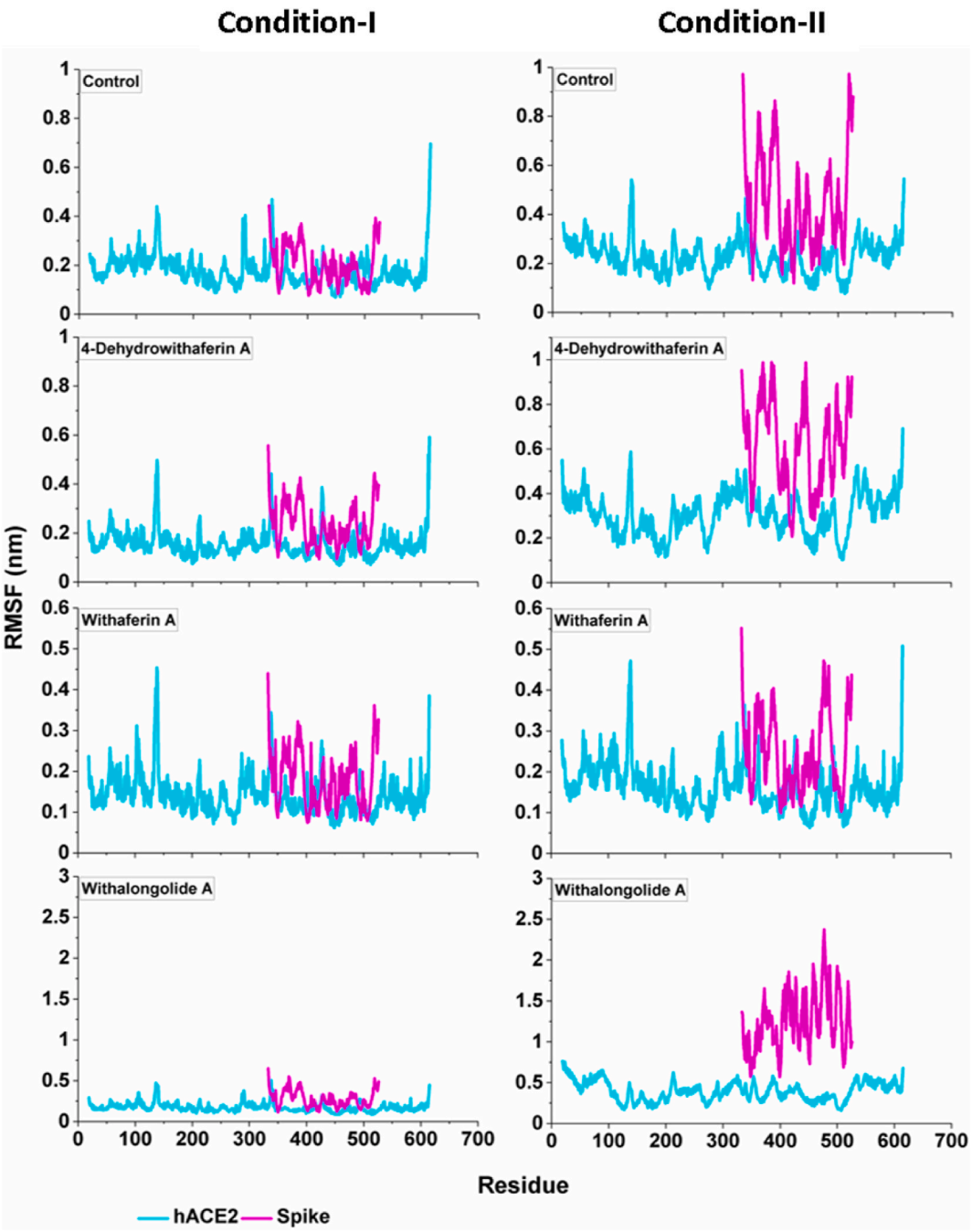

Fig. 3. Root Mean Square Fluctuation (RMSF) of amino acid residues of S-RBD-hACE2-R complex in the presence and absence of ligands under CON–I and CON-II.

THR500-TYR41, THR500-ASP355 and ASN487-TYR83) which are crucial in the formation of the S-RBD and hACE2-R complex, were completely disrupted (Fig. 6A). Additionally, Withalongolide A disrupts the interaction between S-RBD and hACE2-R by forming H-bond with TYR453 (10% HBO), GLN493 (13% HBO), SER494 (16% HBO) and TYR505 (9% HBO) of S-RBD and, LYS31 (11% HBO) and LYS 353 (12% HBO) of hACE2-R (Fig. 6B). Total AAR interactions were reduced to six in the presence of 4-Dehydrowithaferin A. Five AAR interactions were completely disrupted by 0% HBO (TYR505-GLU37, THR500-ASP355, THR500-TYR41, GLY502-LYS353, ASN501-TYR41 and ASN487-GLN29). However, a new interaction between TYR505-LYS553 with HBO of 70% was observed, which was not observed in control (Fig. 6A). 4-Dehydrowithaferin A formed four H-bond with S-RBD [GLN493 (32% HBO), GLU484 (18% HBO), GLY493 (35% HBO), and SER494 (8% HBO)] and one with hACE2-R [LYS353 (10% HBO)]. Though these AAR did not appear in the H-bond pattern of control, by occupying them, 4-Dehydrowithaferin A may disrupt other adjacent AAR interactions (Fig. 6B), thereby decreasing the affinity of S-RBD for hACE2-R. Withaferin A was found to reduce the number of AAR interactions to six, with TYR505-GLU37, LYS417-ASP30 and GLY502-LYS353 exhibiting HBO >70%. Withaferin A is also participates in the formation of H-bonds, interacting with five AAR of S-RBD and one AAR of hACE2-R. The highest of 92% and 70% HBO was observed with GLY496 and GLU484 of S-RBD, respectively (Fig. 6B).

3.3. Analysis of HBO and MMPBSA under CON-II

Under CON-II, in control, although both proteins were initially

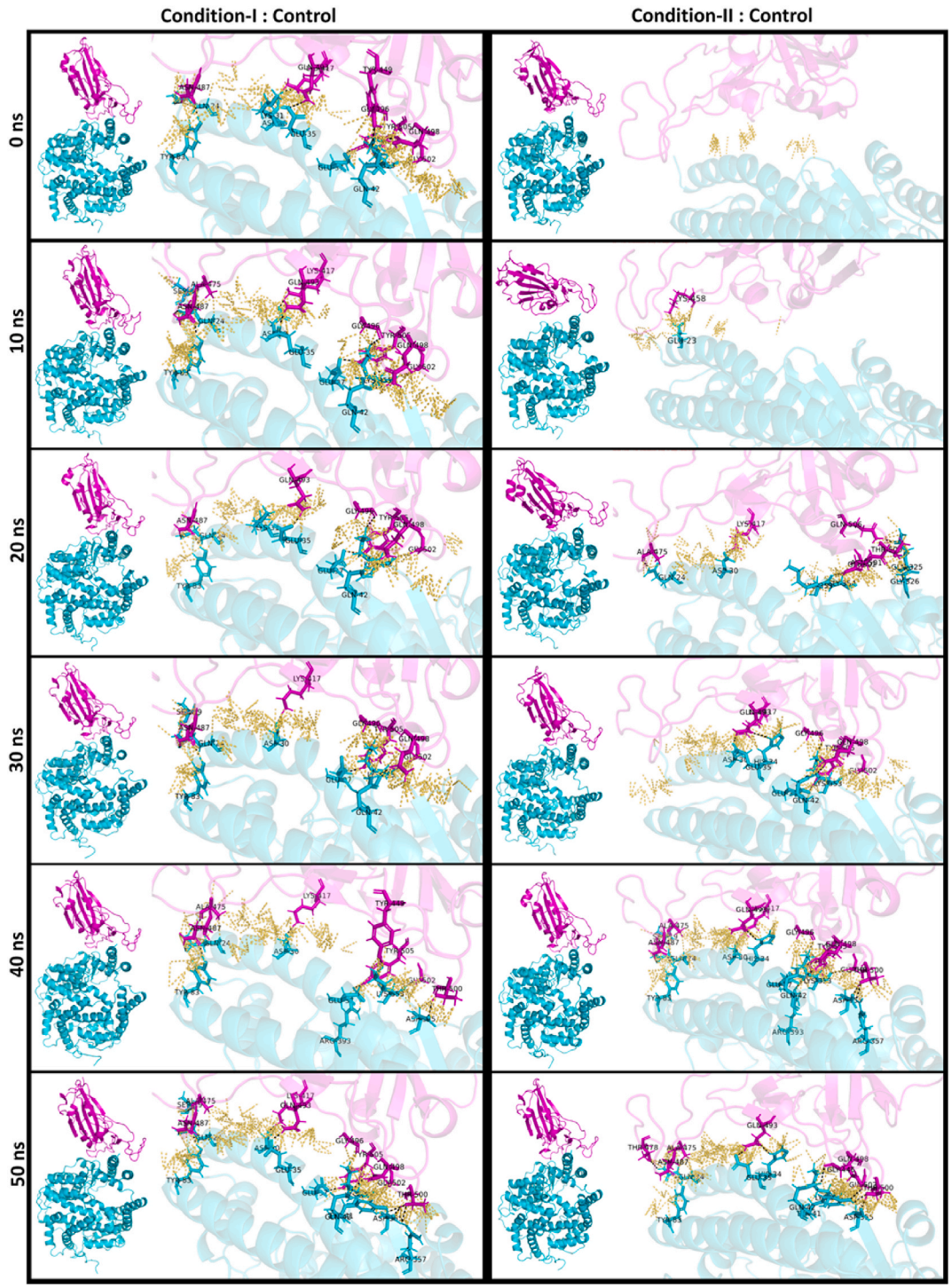

Fig. 4A. Snapshots of MDS at the intervals of 10 ns for control reactions under CON–I and CON-II. In each frame to the left, the S-RBD (magenta color) and hACE2-R (cyan color) and their interacting positions are shown. Close up of protein-protein interface with various interaction was shown on the right side of each frame. Amino acid residues involved in hydrogen bond formation were represented as sticks. Hydrogen bonds are represented as dashed lines in black color, and all other interactions were represented as yellow dash lines.

separated, as the simulation progressed, the interaction between them became stronger due to an increased number of H-bond and other types of molecular interactions (Sup. Fig. 3; Fig. 4A). While the total number of H-bonds (average of 50 ns) between S-RBD and hACE2-R was reduced to 2.0, 3.66, and 1.78 in the presence of 4-Dehydrowithaferin A, Withaferin A and Withalongolide A, respectively, during the simulation period (Sup. Fig. 3). The PPI stabilized with 12 H-bonds near the end of the MDS (last 10 ns) (Fig. 6A). Nine of the restored H-bonds were comparable to the CON–I control (Fig. 6A). When different frames of simulations were analyzed, it was discovered that the alignment of Withalongolide A and 4-Dehydrowithaferin A molecule was parallel to S-RBD, with the ergostane framework was facing towards the C1 of S-RBD and lactone ring is facing towards C3 of S-RBD. At the same time, Withaferin A moved from its original position to C1 and also rotated itself 90°. Interestingly, Withaferin A was found to stabilize the PPI, which was evidenced by decreased free BE from −913.66 kJ/mol

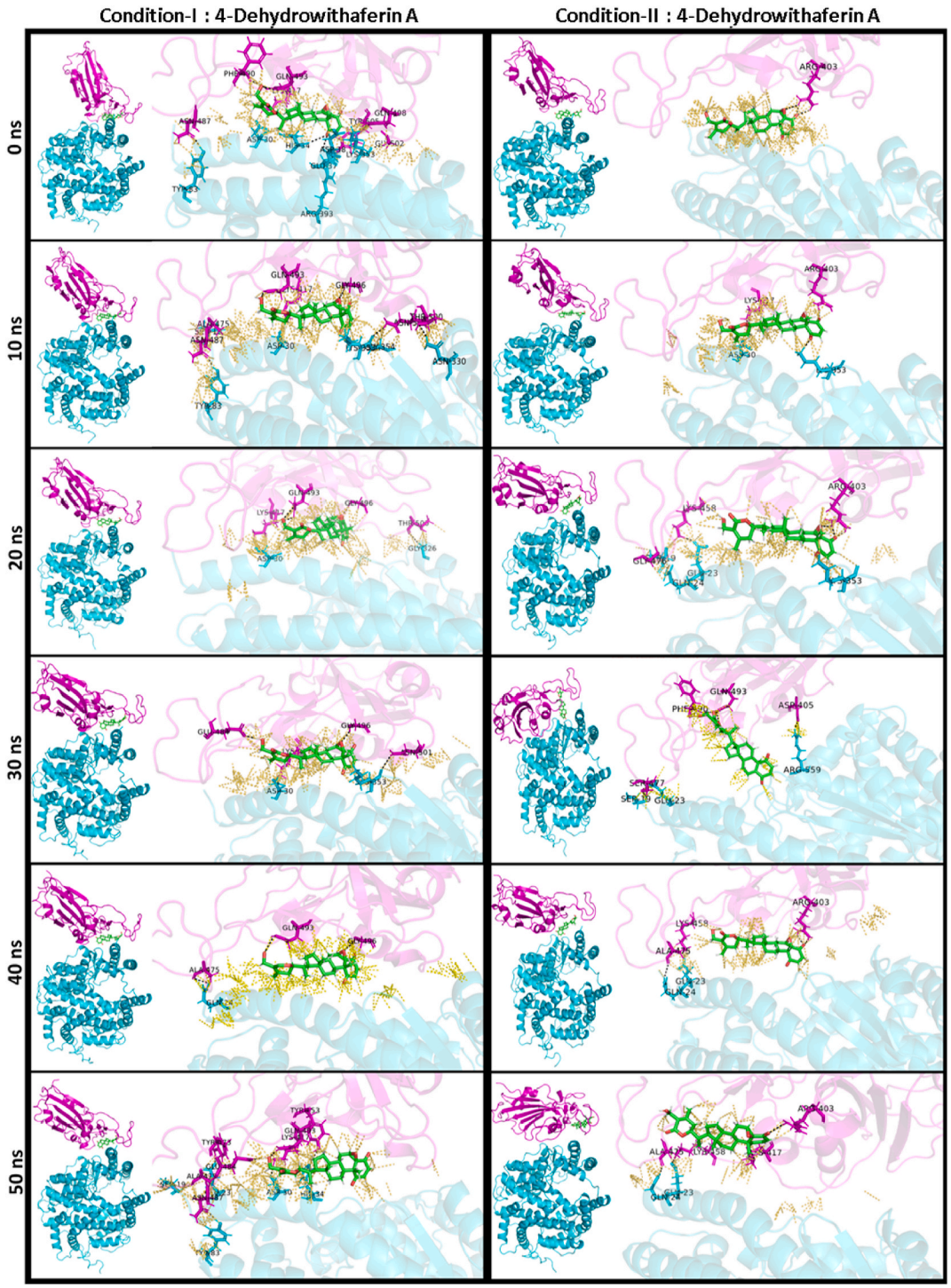

Fig. 4B. Snapshots of MDS at the intervals of 10 ns in the presence of 4-Dehydrowithaferin An under CON–I and CON-II. In each frame to the left, the S-RBD (magenta color) and hACE2-R (cyan color) and their interacting positions are shown. Close up of protein-protein or protein-ligand interaction was shown on the right side of each frame. Amino acid residues involved in hydrogen bond formation are represented as sticks. Hydrogen bonds are represented as dashed lines in black color, and all other interactions are represented as yellow dash lines.

(control) to −1116.55 kJ/mol (Table 1.). Further increase in free BE from −913.66 kJ/mol (control) to −113.69 kJ/mol and −769.62 kJ/mol with Withalongolide A and 4-Dehydrowithaferin, respectively, indicated their potential to reduce S-RBD and hACE2-R affinity. Up to 30 ns, Withalongolide A renders the protein-protein complex highly unstable. Following that, the two proteins were physically separated. Throughout the simulation period, Withalongolide A was found to be strongly bound to the S-RDB, preventing its reunion with hACE2-R (Fig. 4D; Sup. Video 1). Additionally, Withalongolide A formed H-bonds with TYR453 (97% HBO), TYR495 (8% HBO) and GLN493 (8% HBO) of S-RBD. TYR453 of S-RBD is required for binding to HIS34 of hACE2-R, by blocking this AAR; Withalongolide A decreased S-RBD's efficiency, preventing it from attaching to hACE2-R.

Supplementary video related to this article can be found at https://doi.org/10.1016/j.compbiomed.2022.105598

Similarly, 4-Dehydrowithaferin A was discovered to destabilize the

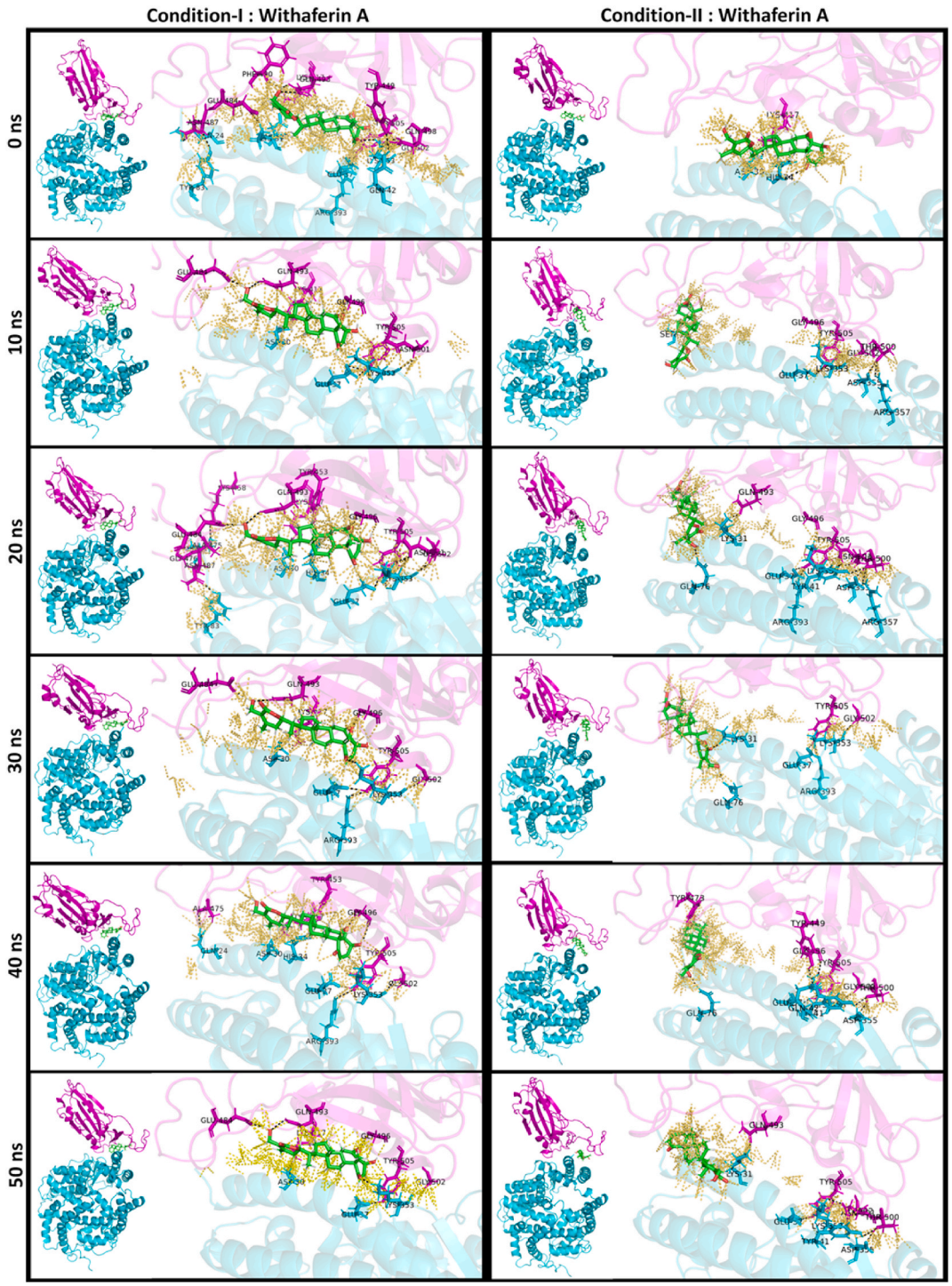

Fig. 4C. Snapshots of MDS at the intervals of 10 ns in the presence of Withaferin An under CON–I and CON-II. In each frame to the left, S-RBD (magenta color) and hACE2-R (cyan color) and their interacting positions are shown. Close up of protein-protein or protein-ligand interactions are shown on the right side of each frame. Amino acid residues involved in hydrogen bond formation are represented as sticks. Hydrogen bonds are represented as dashed lines in black color, and all other interactions are represented as yellow dash lines.

S-RBD and hACE2-R complex, as indicated by S-RBD shifting throughout the simulation. It was immediately apparent that the interaction between S-RBD and hACE2-R had been disrupted. However, both the proteins remained attached via a variety of AAR interactions that may not be involved in normal S-RBD and hACE2-R interactions. Only two H-bonds were observed here, with an HBO percentage of 57% (ALA475-GLN24) and 9% (LYS417-HIS34) (Fig. 6A). Additionally, 4-Dehydrowithaferin A formed two H-bonds [LYS417 (18% HBO) and ARG403 (13% HBO)] with S-RDB and one [LYS31 (23% HBO)] H-bond with hACE2-R (Fig. 6B). Withaferin A was the least capable of disrupting S-RBD and hACE2-R interactions of the three SL studied. Five H-bonds were identified here, with GLY502-LYS353, THR500-ASP355 and TYR505-GLU37 exhibiting >80% HBO (Fig. 6A). Withaferin A itself formed an H-bond with TYR473 (6% HBO) of S-RBD and GLN76 (10% HBO) of hACE2-R, respectively (Fig. 6B).

Under both CON–I and CON-II, the interaction of ligand with protein

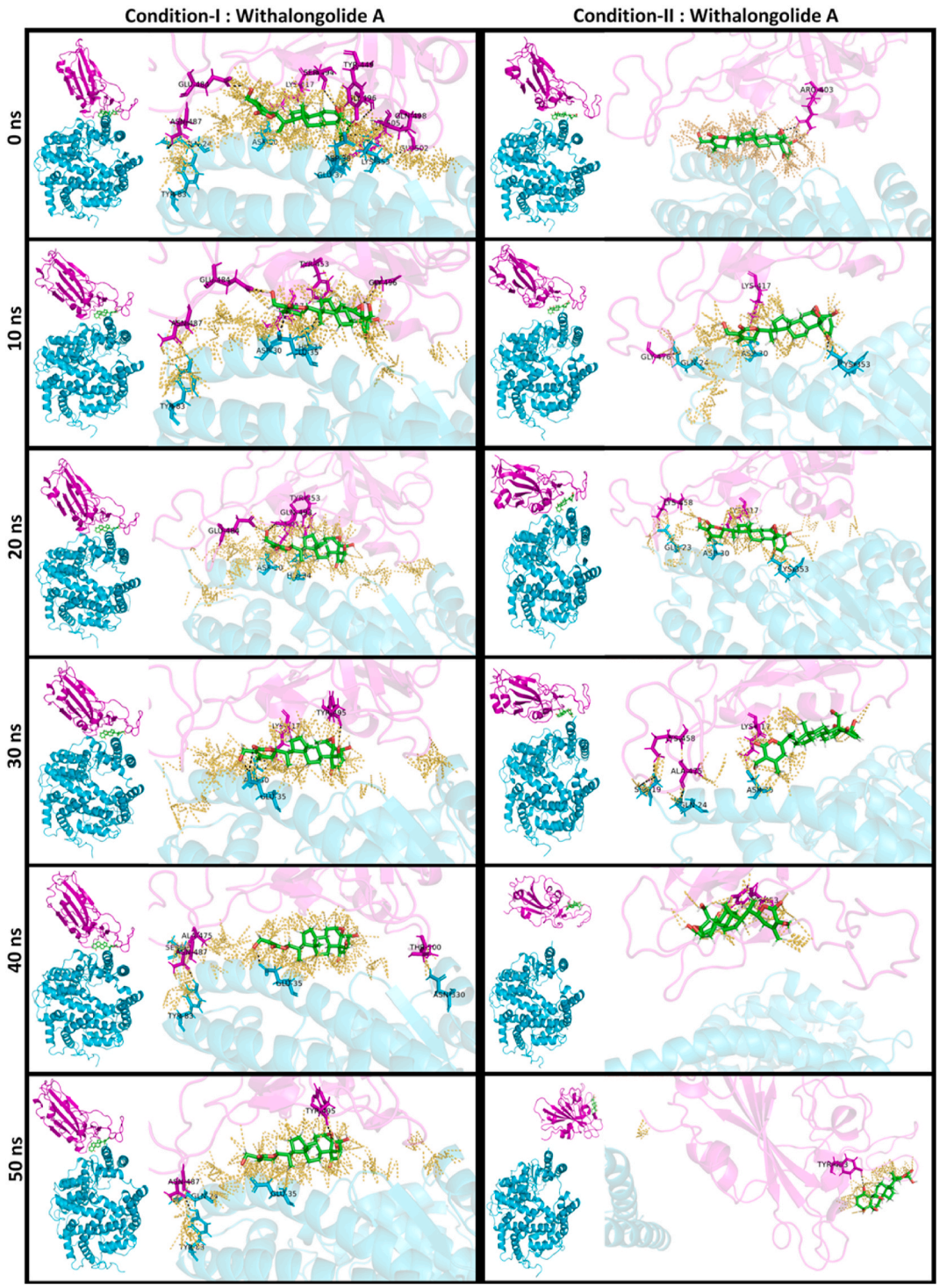

Fig. 4D. Snapshot of MDS at the intervals of 10 ns in the presence of Withalongolide An under CON–I and CON-II. In each frame to the left, S-RBD (magenta color) and hACE2-R (cyan color) and their interacting positions are shown. Close up of protein-protein or protein-ligand interactions were shown on the right side of each frame. Amino acid residues involved in hydrogen bond formation are represented as sticks. Hydrogen bonds are represented as dashed lines in black color, and all other interactions are represented as yellow dash lines.

resulted in the formation of primarily H-bonds between the oxygen and hydroxyl groups on the cyclohexane A ring on the ergostane frame and the unsaturated lactone ring. Though all three selected SL molecules are structurally similar (Sup. Fig. 2), the minor difference in the oxygen atom and hydroxyl group distribution on the cyclohexane A and B rings appears to play a role in their differential ability to interact with S-RBD and hACE2-R. The current study demonstrated the ability of two PSM (Withalongolide A and 4-Dehydrowithaferin A) to disrupt S-RBD and hACE2-R interactions, thereby preventing a virus's early recognition of host cell.

Additionally, the three SL studies met Lipinski's rule of drug-likeness, with a bioavailability score of 0.55. All SL exhibited low water solubility high intestinal absorption, and could not cross the blood-brain barrier (BBB). While SLs were identified as a p-glycoprotein I and II inhibitors and were negative for CYP1A2, CYP2C19, CYP2C9, CYP2D6 and CYP3AY inhibition. Only Withalongolide A was found to be

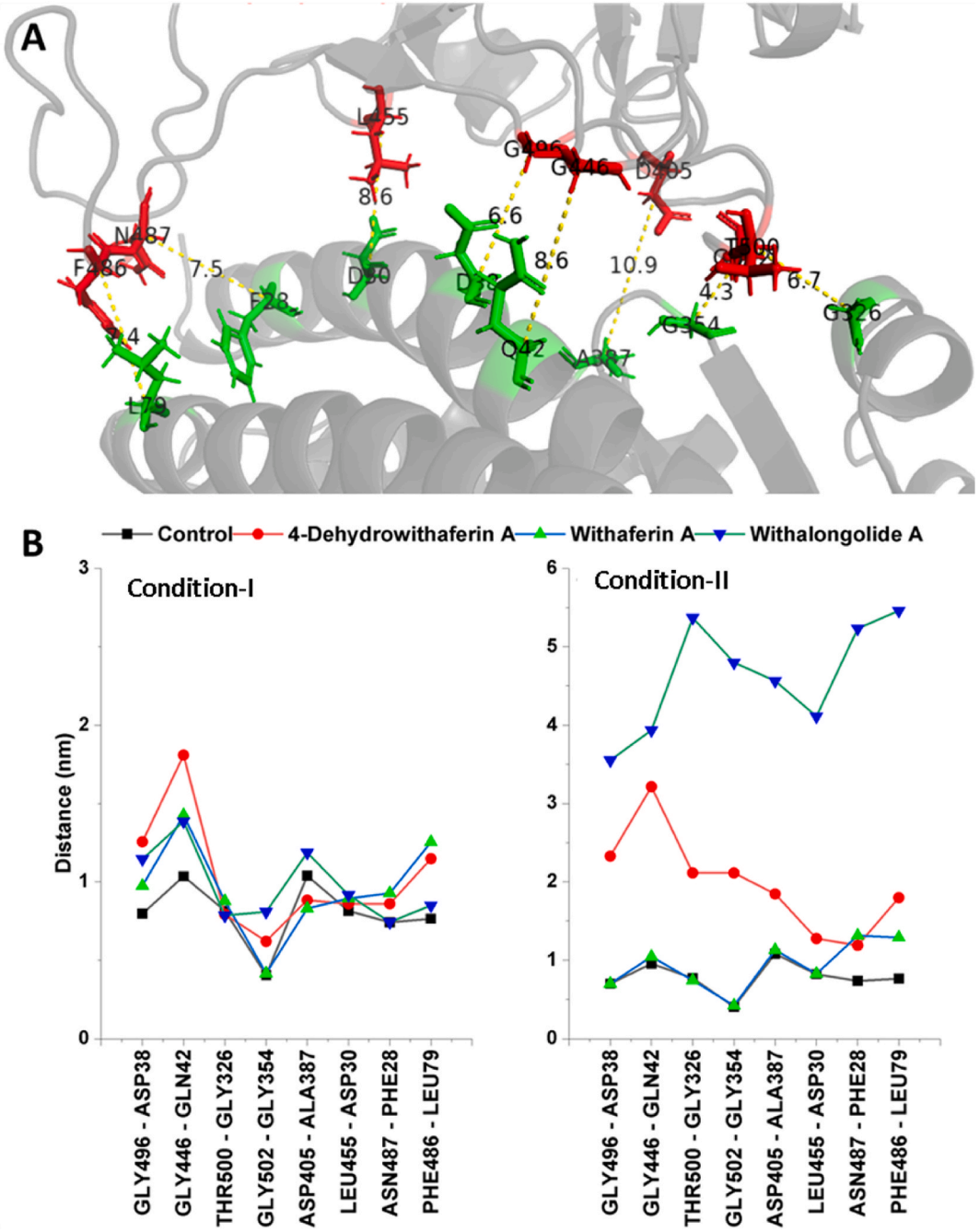

Fig. 5. A. The physical location of eight amino acid combinations distributed across the S-RBD and hACE2-R interacting surface used in the present study to monitor the distance between S-RBD-hACE2-R complex during the MDS process. B. Average distance between the selected eight amino acid (C_α atoms) combinations measured during the last 10 ns MDS under CON–I and CON-II indicating distance between S-RBD and hACE2-R.

toxic to the liver (Sup. Tables 1 and 2).

In a similar attempt, Garcia et al. [11] reported the PPI disrupting the ability of plicamycin in SARS-CoV-2 pathogenesis. The distance between selected protein points increased from 44 Å to 49 Å in the presence of plicamycin. Additionally, the destabilization of the PPI was demonstrated by a decrease in the free energy profile from 3 kcal/mol (native complex) to 2.1 kcal/mol (plicamycin complex) and a decrease in the number of H-bond formations between the proteins. However, several small molecules have previously been shown to disrupt the interaction between S-RBD and hACE2-R. They were limited to MD, and their capabilities were not evaluated through MDS. Our approach of MDS in this study instilled more confidence in the SL, allowing them to be considered for additional *in-vitro* and *in-vivo* studies. Balakrishna et al. [38] conducted a similar computational study and discovered that SL (Withanone) molecules have the potential to disrupt the S-RBD and hACE2-R interaction. Further, an *in-vitro* study found extracts rich in withanone from *Withania somnifera*, reduced the human-like pathological responses induced in humanized zebrafish by SARS-CoV-2 recombinant spike protein. In a similar attempt, DYGAVNEVK, a peptide derived from fruit bromelain, was observed to inhibit the interaction between S-RBD derived from different variants of SARS-CoV-2 and hACE2. The peptide interacted with the critical amino acid involved in the attachment of S-RBD and hACE2, and PPI destabilization was evidenced by a decrease in binding free energy [74]. Basu et al. [75] observed that the PPI of S-RBD and hACE2 was significantly reduced by a hesperidin (flavanone glycoside) by increasing the binding energy

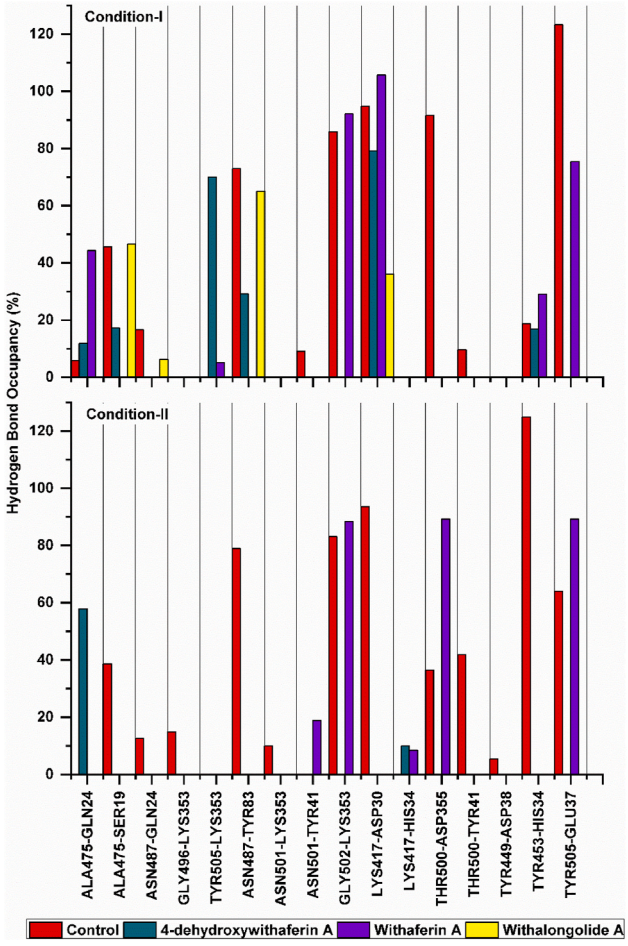

Fig. 6A. Hydrogen bond occupancy between the protein-protein interface amino acid residues (S-RBD ↔ hACE2-R) in the presence and absence of ligands under CON–I and CON-II.

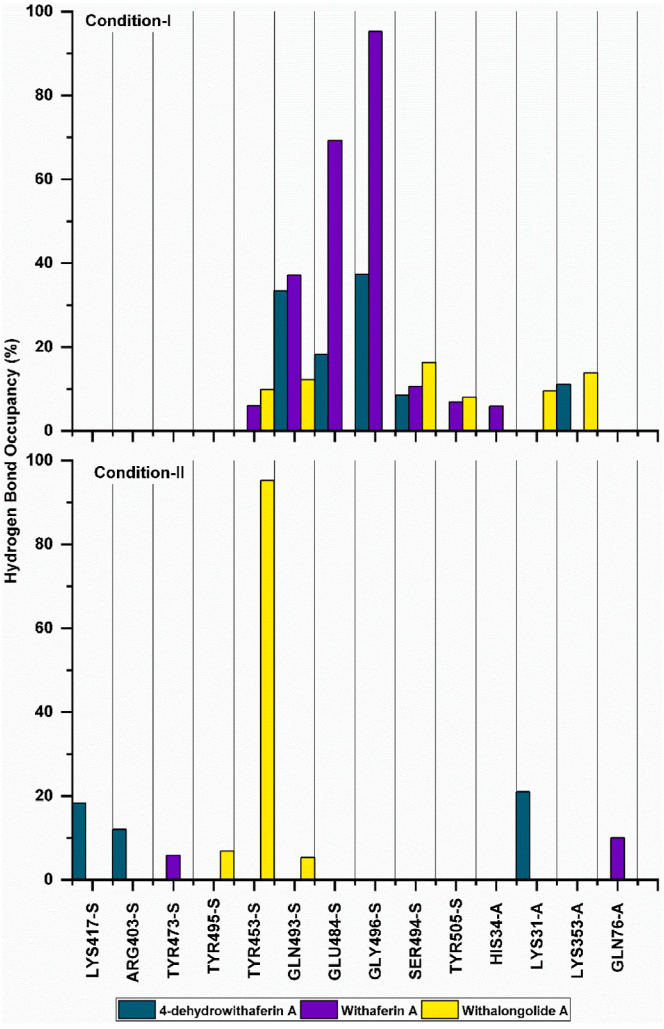

Fig. 6B. Hydrogen bond occupancy between the ligand ↔ S-RBD and ligand ↔ hACE2-R under CON–I and CON-II. Letter S and A in front of amino acid residue on x axis represents the S-RBD and hACE2-R, respectively.

from −779.8 kcal/mol (control) to −677.6 kcal/mol.

4-Dehydrowithaferin A destabilized the PPI under CON–I. While Withalongolide A completely separates two proteins under CON-II, and ligand remains attached to the S-RBD throughout the simulation. 4-Dehydrowithaferin A and Withalongolide A exhibit strong interactions with S-RBD, indicating that they have a negligible effect on the structural integrity and function of the host protein – hACE2. Also, the present study established for the first time, to our knowledge and that of the literature, the ability of SLs to disrupt PPI of S-RBD-hACE2-R complex via MDS. As a result, these molecules can be further investigated to their full potential through *in-vitro, in-vivo,* and clinical studies. Due to the fact that these molecules are abundant in *Withania somnifera,* a well-known medicinal plant used in the Indian Ayurveda system, they can be introduced into the medicinal system with minimal effort to manage COVID-19. While our study focused on wild type SARS-CoV-2, the same approach could be used to screen the aforementioned molecules or secondary metabolites from other sources against emerging variants with increased transmissibility and virulence.

Author contributions

Ajay Yadav and Monu Dinesh Ojha-investigation, writing, review, validation, visualization, data curation.

Prof. Hariprasad P.-conceptualization, resources, supervision, review, data curation.

Declaration of competing interest

All authors declares no conflict of interest.

Acknowledgement

The authors wish to express their gratitude to the IIT Delhi HPC facility for computational resources and the Director, IIT Delhi, for the immense support.

Appendix A. Supplementary data

Supplementary data to this article can be found online at https://doi.org/10.1016/j.compbiomed.2022.105598.

References

[1] R. J de Groot, R. Baric, L. Enjuanes, A.E. Gorbalenya, K.V. Holmes, S. Perlman, Family Coronaviridae. Virus Taxonomy: Classification and Nomenclature of Viruses: Ninth Report of the International Committee on Taxonomy of Viruses, 2011.
[2] https://covid19.who.int/ (5th January 2022, date last accessed).
[3] https://www.who.int/en/activities/tracking-SARS-CoV-2-variants/ (10th January 2022, date last accessed).
[4] J. Machhi, J. Herskovitz, A.M. Senan, D. Dutta, B. Nath, M.D. Oleynikov, The natural history, pathobiology, and clinical manifestations of SARS-CoV-2

infections, J. Neuroimmune Pharmacol. 15 (2020) 359–386. https://doi:10.1007/s11481-020-09944-5.
[5] A.A.T. Naqvi, K. Fatima, T. Mohammad, et al., Insights into SARS-CoV-2 genome, structure, evolution, pathogenesis and therapies: structural genomics approach, Biochim. Biophys. Acta (BBA) - Mol. Basis Dis. 1866 (2020), 165878, https://doi.org/10.1016/j.bbadis.2020.165878.
[6] F.A. Rabi, M.S. Al Zoubi, G.A. Kasasbeh, et al., SARS-CoV-2 and coronavirus disease 2019: what we know so far, Pathogens 9 (2020) 231, https://doi.org/10.3390/pathogens9030231.
[7] A.C. Walls, Y.J. Park, M.A. Tortorici, A. Wall, A.T. McGuire, D. Veesler, Structure, function, and antigenicity of the SARS-CoV-2 spike glycoprotein, Cell 181 (2020) 281–292, https://doi.org/10.1016/j.cell.2020.02.058.
[8] K.G. Anderson, A. Rambaut, W.I. Lipkin, E.C. Holmes, R.F. Garry, The proximal origin of SARS-CoV-2, Nat. Med. 26 (2020) 450–452, https://doi.org/10.1038/s41591-020-0820-9.
[9] J. Lan, J. Ge, J. Yu, S. Shan, H. Zhou, S. Fan, Q. Zhang, X. Shi, Q. Wang, L. Zhang, X. Wang, Structure of the SARS-CoV-2 spike receptor-binding domain bound to the ACE2 receptor, Nature 581 (2020) 215–220, https://doi.org/10.1038/s41586-020-2180-5.
[10] I. Khatri, F.J. Staal, J.J. Van Dongen, Blocking of the high-affinity interaction-synapse between SARS-CoV-2 spike and human ACE2 proteins likely requires multiple high-affinity antibodies: an immune perspective, Front. Immunol. 11 (2020) 2258, https://doi.org/10.3389/fimmu.2020.570018.
[11] C. García-Iriepa, C. Hognon, A. Francés-Monerris, I. Iriepa, T. Miclot, G. Barone, A. Monari, M. Marazzi, Thermodynamics of the interaction between the spike protein of severe acute respiratory syndrome coronavirus-2 and the receptor of human angiotensin-converting Enzyme 2. Effects of possible ligands, J. Phys. Chem. Lett. 11 (2020) 9272–9281, https://doi.org/10.1021/acs.jpclett.0c02203.
[12] M. Sokolowska, Outsmarting SARS-CoV-2 by empowering a decoy ACE2, Sig, Transduct. Target Ther. 5 (2020) 260, https://doi.org/10.1038/s41392-020-00370-w.
[13] Therapeutics and COVID-19: Living Guideline. https://www.who.int/publications/i/item/WHO-2019-nCoV-therapeutics-2021.3 (10th January 2022, date last accessed).
[14] Coronavirus (COVID-19) | Drugs. https://www.fda.gov/drugs/emergency-preparedness-drugs/coronavirus-covid-19-drugs. (10th January 2022, date last accessed).
[15] https://covid19.trackvaccines.org/agency/who/.(10th January 2022, date last accessed).
[16] L.T. Lin, W.C. Hsu, C.C. Lin, Antiviral natural products and herbal medicines, J. Tradl. Complement. Med. 4 (2014) 24–35, https://doi.org/10.4103/2225-4110.124335.
[17] J.P. Martinez, F. Sasse, M. Brönstrup, J. Diez, A. Meyerhans, Antiviral drug discovery: broad-spectrum drugs from nature, Nat. Prod. Rep. 32 (2015) 29–48, https://doi.org/10.1039/c4np00085d.
[18] I. Aanouz, A. Belhassan, K.E. Khatabi, T. Lakhlifi, M. El-Ldrissi, M. Bouachrine, Moroccan medicinal plants as inhibitors of COVID-19: computational investigations, J. Biomol. Struct. Dyn. 39 (2020) 2971–2979, https://doi.org/10.1080/07391102.2020.1758790.
[19] A.A. Elfiky, Natural products may interfere with SARS-CoV-2 attachment to the host cell, J. Biomol. Struct. Dynam. 39 (2021) 3194–3203, https://doi.org/10.1080/07391102.2020.1761881.
[20] X. Du, L. Shi, W. Cao, B. Zuo, A. Zhou, Add-on effect of Chinese herbal medicine in the treatment of mild to moderate COVID-19: a systematic review and meta-analysis, PLoS One 16 (2021), e0256429, https://doi.org/10.1371/journal.pone.0256.
[21] L. Luo, J. Jiang, C. Wang, M. Fitzgerald, W. Hu, Y. Zhou, H. Zhang, S. Chen, Analysis on herbal medicines utilized for treatment of COVID-19, Acta Pharm. Sin. B 10 (2020) 1192–1204. https://doi: 10.1016/j.apsb.2020.05.007.
[22] D. Silveira, J.M. Prieto-Garcia, F. Boylan, O. Estrada, Y.M. Fonseca-Bazzo, C. M. Jamal, P.O. Magalhães, E.O. Pereira, M. Tomczyk, M. Heinrich, COVID-19: is there evidence for the use of herbal medicines as adjuvant symptomatic therapy? Front. Pharmacol. 11 (2020) 81840, https://doi.org/10.3389/fphar.2020.581840.
[23] P. Kanjanasirirat, A. Suksatu, S. Manopwisedjaroen, B. Munyoo, P. Tuchinda, K. Jearawuttanakul, S. Seemakhan, S. Charoensutthivarakul, P. Wongtrakoongate, N. Rangkasenee, S. Pitiporn, N. Waranuch, N. Chabang, P. Khemawoot, K. Sa-Ngiamsuntorn, Y. Pewkliang, P. Thongsri, S. Chutipongtanate, S. Hongeng, S. Borwornpinyo, A. Thitithanyanont, High-content screening of Thai medicinal plants reveals Boesenbergia rotunda extract and its component Panduratin A as anti-SARS-CoV-2 agents, Sci. Rep. 17 (2020) 19963. https://doi: 10.1038/s41598-020-77003-3.
[24] I.E. Orhan, F.S. Senol Deniz, Natural products as potential leads against coronaviruses: could they be encouraging structural models against SARS-CoV-2? Nat. Prod. Bioprospect. 10 (2020) 171–186. https://doi: 10.1007/s13659-020-00250-4.
[25] R. Xiang, Z. Yu, Y. Wang, L. Wang, S. Huo, Y. Li, R. Liang, Q. Hao, T. Ying, Y. Gao, F. Yu, Recent advances in developing small-molecule inhibitors against SARS-CoV-2, Acta Pharm. Sin. B (2021), https://doi.org/10.1016/j.apsb.2021.06.016.
[26] C. Yang, X. Pan, X. Xu, C. Cheng, Y. Huang, L. Li, S. Jiang, W. Xu, G. Xiao, S. Liu, Salvianolic acid C potently inhibits SARS-CoV-2 infection by blocking the formation of six-helix bundle core of spike protein, Signal Transduct. Targeted Ther. 6 (2020) 220. https://doi: 10.1038/s41392-020-00325-1.
[27] C.Z. Chen, M. Xu, M. Pradhan, K. Gorshkov, J.D. Petersen, M.R. Straus, W. Zhu, P. Shinn, H. Guo, M. Shen, C. Klumpp-Thomas, S.G. Michael, J. Zimmerberg, W. Zheng, G.R. Whittaker, Identifying SARS-CoV-2 entry inhibitors through drug repurposing screens of SARS-S and MERS-S pseudotyped particles, ACS Pharmacol. Transl Sci. 19 (2020) 1165–1175. https://doi: 10.1021/acsptsci.0c00112.
[28] S. Huang, Y. Liu, Y. Zhang, R. Zhang, C. Zhu, L. Fan, G. Pei, B. Zhang, Y. Shi, Baicalein inhibits SARS-CoV-2/VSV replication with interfering mitochondrial oxidative phosphorylation in a mPTP dependent manner, Signal Transduct. Targeted Ther. 13 (2020) 266. https://doi: 10.1038/s41392-020-00353-x.
[29] W.D. Jang, S. Jeon, S. Kim, S.Y. Lee, Drugs repurposed for COVID-19 by virtual screening of 6,218 drugs and cell-based assay, Proc. Natl. Acad. Sci. U. S. A. 118 (30) (2021 Jul 27), e2024302118. https://doi: 10.1073/pnas.2024302118.
[30] L. Huang, T.T. Yuen, Z. Ye, S. Liu, G. Zhang, H. Chu, J. Yue, Berbamine inhibits SARS-CoV-2 infection by compromising TRPMLs-mediated endolysosomal trafficking of ACE2, Signal Transduct. Targeted Ther. 6 (2021) 168. https://doi: 10.1038/s41392-021-00584-6.
[31] M.H. Mirjalili, E. Moyano, M. Bonfill, R.M. Cusido, J. Palazón, Steroidal lactones from Withania somnifera, an ancient plant for novel medicine, Molecules 14 (2009) 2373–2393. https://doi:10.3390/molecules14072373.
[32] C. Scarfiotti, F. Fabris, B. Cestaro, A. Giuliani, Free radicals, atherosclerosis, ageing and related dysmetabolic pathologies: pathological and clinical aspects, Eur. J. Cancer Prev. 6 (1997) S31–S36. https://doi: 10.1097/00008469-199703001-00007.
[33] S. Hemalatha, A.K. Wahi, P.N. Singh, J.P. Chansouria, Hypolipidemic activity of aqueous extract of Withania coagulans dunal in Albino rats, Phytother Res. 20 (2006) 614–617. https://doi: 10.1002/ptr.1916.
[34] B. Andallu, B. Radhika, Hypoglycemic, diuretic and hypocholesterolemic effect of winter cherry (Withania somnifera, Dunal) root, Indian J. Exp. Biol. 38 (2000) 607–609.
[35] P.S. Naidu, A. Singh, S.K. Kulkarni, Effect of Withania somnifera root extract on reserpine induced orofacial dyskinesia and cognitive dysfunction, Phytother Res. 20 (2006) 140–146. https://doi: 10.1002/ptr.1823.
[36] A. Mahima, A. Rahal, R. Deb, S.K. Latheef, H. Samad, R. Tiwari, A.K. Verma, A. Kumar, K. Dhama, Immunomodulatory and therapeutic potentials of herbal, traditional/indigenous and ethnoveterinary medicines, Pakistan J. Biol. Sci. 15 (2012). https://doi: 10.3923/pjbs.2012.754.774, 754-74.
[37] K. Dhama, S. Chakraborty, R. Tiwari, Panchgavya therapy (Cowpathy) in safeguarding health of animals and humans: a review, Res. Opin. Anim. Vet. Sci. 3 (2013) 170–178.
[38] A. Balkrishna, S. Pokhrel, H. Singh, M. Joshi, V.P. Mulay, S. Haldar, A. Varshney, A, Withanone from Withania somnifera attenuates SARS-CoV-2 RBD and host ACE2 interactions to rescue spike protein induced pathologies in humanized zebrafish model, Drug Des. Dev. Ther. 15 (2021) 1111–1133, https://doi.org/10.2147/DDDT.S292805.
[39] V. Kumar, J.K. Dhanja, P. Bhargava, A. Kaul, J. Wang, H. Zhang, S.C. Kaul, R. Wadhwa, D. Sundar, Withanone and withaferin-A are predicted to interact with transmembrane protease serine 2 (TMPRSS2) and block entry of SARS-CoV-2 into cells, J. Biomol. Struct. Dyn. 16 (2020) 1–13, https://doi.org/10.1080/07391102.2020.1775704.
[40] V. Chandel, S. Raj, B. Rathi, D. Kumar, In silico identification of potent FDA approved drugs against coronavirus covid-19 main protease: a drug repurposing approach, Chemical Biology Letters 7 (2020) 166–175.
[41] B. Khan, S.F. Ahmad, S. Bani, Augmentation and proliferation of T lymphocytes and Th-1 cytokines by Withania somnifera in stressed mice, Int. Immunopharm. 6 (2006) 1394–1403. https://doi: 10.1016/j.intimp.2006.04.001.
[42] F. Malik, J. Singh, A. Khajuria, K.A. Suri, N.K. Satti, S. Singh, M.K. Kaul, A. Kumar, A. Bhatia, G.N. Qazi, A standardized root extract of Withania somnifera and its major constituent withanolide-A elicit humoral and cell-mediated immune responses by up regulation of Th1-dominant polarization in BALB/c mice, Life Sci. 80 (2007) 1525–1538. https://doi: 10.1016/j.lfs.2007.01.029.
[43] M. Sosnowski, J. Krzywanski, R. Ščurek, Artificial intelligence and computational methods in the modeling of complex systems, Entropy (Basel, Switzerland) 23 (2021) 586, https://doi.org/10.3390/e23050586.
[44] A. Basu, A. Sarkar, U. Maulik, Molecular docking study of potential phytochemicals and their effects on the complex of SARS-CoV2 spike protein and human ACE2, Sci. Rep. 10 (2020) 17699, https://doi.org/10.1038/s41598-020-74715-4.
[45] H. Puttaswamy, H.G. Gowtham, M.D. Ojha, A. Yadav, G. Choudhir, V. Raguraman, B. Kongkham, K. Selvaraju, S. Shareef, P. Gehlot, F. Ahamed, In silico studies evidenced the role of structurally diverse plant secondary metabolites in reducing SARS-CoV-2 pathogenesis, Sci. Rep. 10 (2020) 20584, https://doi.org/10.1038/s41598-020-77602-0.
[46] J. Fuska, A. Fusková, J.P. Rosazza, A.W. Nicholas, Novel cytotoxic and antitumor agents. IV. Withaferin A: relation of its structure to the in vitro cytotoxic effects on P388 cells, Neoplasma 31 (1984) 31–36.
[47] E.F. Pettersen, T.D. Goddard, C.C. Huang, G.S. Couch, D.M. Greenblatt, E.C. Meng, T.E. Ferrin, UCSF chimera - a visualization system for exploratory research and analysis, J. Comput. Chem. 25 (2004) 1605–1612, https://doi.org/10.1002/jcc.20084.
[48] N. Guex, M.C. Peitsch, SWISS-MODEL and the Swiss-Pdb Viewer: an environment for comparative protein modeling, Electrophoresis 18 (1997) 2714–2723, https://doi.org/10.1002/elps.1150181505.
[49] R.E. Amaro, J. Baudry, J. Chodera, Ö. Demir, J.A. McCammon, Y. Miao, J.C. Smith, Ensemble docking in drug discovery, Biophys. J. 114 (2018) 2271–2278, https://doi.org/10.1016/j.bpj.2018.02.038.
[50] M.J. Abraham, J.E. Gready, Optimization of parameters for molecular dynamics simulation using smooth particle-mesh Ewald in GROMACS 4.5, J. Comput. Chem. 32 (2011) 2031–2040, https://doi.org/10.1002/jcc.21773.

[51] H. Berendsen, D. Van Der Spoel, R. Van Drunen, GROMACS: a message-passing parallel molecular dynamics implementation, Comput. Phys. Commun. 91 (1995) 43–56. https://doi: 10.1016/0010-4655(95)00042-E.
[52] D. Van Der Spoel, E. Lindahl, B. Hess, G. Groenhof, A.E. Mark, H.J. Berendsen, GROMACS: fast, flexible, and free, J. Comput. Chem. 26 (2005) 1701–1718, https://doi.org/10.1002/jcc.20291.
[53] B.R. Brooks, C.L. Brooks III, A.D. Mackerell, et al., CHARMM: the biomolecular simulation program, J.Comp. Chem. 30 (2009) 1545–1615, https://doi.org/10.1002/jcc.21287.
[54] V. Zoete, M.A. Cuendet, A. Grosdidier, O. Michielin, SwissParam, a fast force field generation tool for small organic molecules, J. Comput. Chem. 32 (2011) 2359–2368, https://doi.org/10.1002/jcc.21816.
[55] W.L. Jorgensen, J. Chandrasekhar, J.D. Madura, R.W. Impey, M.L. Klein, Comparison of simple potential functions for simulating liquid water, J. Chem. Phys. 79 (1983) 926–935, https://doi.org/10.1063/1.445869.
[56] L. Verlet, Computer 'experiments' on classical fluids. I. Thermodynamical properties of Lennard-Jones molecules, Phys. Rev. 159 (1967) 98–103, https://doi.org/10.1103/PhysRev.159.98.
[57] U. Essmann, L. Perera, M.L. Berkowitz, T. Darden, H. Lee, L.G. Pedersen, A smooth particle mesh Ewald method, J. Chem. Phys. 103 (1995) 8577–8593, https://doi.org/10.1063/1.470117.
[58] B. Hess, H. Bekker, H.J.C. Berendsen, et al., LINCS: a linear constraint solver for molecular simulations, J. Comput. Chem. 18 (1997) 1463–1472, https://doi.org/10.1002/(SICI)1096-987X(199709)18:123.0.CO;2-H.
[59] B. Hess, P-LINCS: a Parallel linear constraint solver for molecular simulation, J. Chem. Theor. Comput. 4 (2008) 116–122, https://doi.org/10.1021/ct700200b.
[60] M. Parrinello, A. Rahman, Polymorphic transitions in single crystals: a new molecular dynamics method, J. Appl. Phys. 52 (1981) 7182–7190.
[61] H.J.C. Berendsen, J.P.M. Postma, W.F. VanGunsteren, et al., Molecular dynamics with coupling to an external bath, J. Chem. Phys. 81 (1984) 3684–3690, https://doi.org/10.1063/1.448118.
[62] R. Kumari, R. Kumar, A. Lynn, g_mmpbsa - a GROMACS tool for high-throughput MM-PBSA calculations, J. Chem. Inf. Model. 54 (2014) 1951–1962, https://doi.org/10.1021/ci500020m.
[63] N.A. Baker, D. Sept, S. Joseph, M.J. Holst, J.A. McCammon, Electrostatics of nanosystems: application to microtubules and the ribosome, Proc. Natl. Acad. Sci. U. S. A 98 (2001) 10037–10041, https://doi.org/10.1073/pnas.
[64] Origin (Pro), Version Number (e.g. "Version 2021b"). OriginLab Corporation, Northampton, MA, USA.
[65] W. Humphrey, A. Dalke, K. Schulten, VMD - visual molecular dynamics, J. Mol. Graph. 14 (1996) 33–38, https://doi.org/10.1016/0263-7855(96)00018-5.
[66] A. Daina, O. Michielin, V. Zoete, SwissADME: a free web tool to evaluate pharmacokinetics, drug-likeness and medicinal chemistry friendliness of small molecules, Sci. Rep. 7 (2017) 42717, https://doi.org/10.1038/srep42717.
[67] D.E. Pires, T.L. Blundell, D.B. Ascher, pkCSM: predicting small-molecule pharmacokinetic and toxicity properties using graph-based signatures, J. Med. Chem. 58 (2015) 4066–4072, https://doi.org/10.1021/acs.jmedchem.5b00104.
[68] E.M.K. Wijeratne, Y. Xu, M.T. Marron, et al., Isolation and synthesis of analogs of the anticancer natural product withaferin A for structure-activity relationship studies, in: Forty Second Western Regional Meeting of the American Chemical Society, Las Vegas, NV, United States, 2008, pp. 23–27. Abstracts.
[69] H. Matsuda, T. Murakami, A. Kishi, M. Yoshikawa, Structures of withanosides I, II, III, IV, V, VI, and VII, new withanolide glycosides, from the roots of Indian Withania somnifera Dunal. and inhibitory activity for tachyphylaxis to clonidine in isolated Guinea-pig ileum, Bioorg. Med. Chem. 9 (2001) 1499–1507. https://doi: 10.1016/s0968-0896(01)00024-4.
[70] A.K. Samadi, Potential anticancer properties and mechanisms of action of withanolides, Enzymes 37 (2015) 73–94. https://doi: 10.1016/bs.enz.2015.05.002.
[71] F. Aqil, R. Munagala, A.K. Agrawal, R. Gupta, Anticancer Phytocompounds: Experimental and Clinical Updates, New Look to Phytomedicine, 2019, pp. 237–272.
[72] N.R. Perestelo, G.G. Llanos, C.P. Reyes, A. Amesty, K. Sooda, S. Afshinjavid, I. A. Jiménez, F. Javid, F, I.L. Bazzocchi, Expanding the chemical space of withaferin A by incorporating silicon to improve its clinical potential on human ovarian carcinoma cells, J. Med. Chem. 62 (2019) 4571–4585. https://doi: 10.1021/acs.jmedchem.9b00146.
[73] H.F. Motiwala, J. Bazzill, A. Samadi, H. Zhang, B.N. Timmermann, M.S. Cohen, J. Aubé, Synthesis and cytotoxicity of semisynthetic Withalongolide A analogues, ACS Med. Chem. Lett. 14 (2013) 1069–1073. https://doi: 10.1021/ml400267q.
[74] T.E. Tallei, Fatimawali, A.A. Adam, M.M. Elseehy, A.M. El-Shehawi, E. A. Mahmoud, et al., Fruit bromelain-derived peptide potentially restrains the attachment of SARS-CoV-2 variants to hACE2: a pharmacoinformatics approach, Molecules 27 (2022) 260. https://doi: 10.3390/molecules27010260.
[75] A. Basu, A. Sarkar, U. Maulik, Molecular docking study of potential phytochemicals and their effects on the complex of SARS-CoV2 spike protein and human ACE2, Sci. Rep. 10 (2020) 17699, https://doi.org/10.1038/s41598-020-74715-4.